

Highlights from the STAR experiment

Sooraj Radhakrishnan for the STAR Collaboration*

Lawrence Berkeley National Laboratory, Berkeley, CA, 94720

E-mail: skradhakrishnan@lbl.gov

Studies of the Quark Gluon Plasma (QGP) with hard and electromagnetic probes are a major focus of the STAR experiment at the Relativistic Heavy Ion Collider. The Heavy Flavor Tracker installed at STAR for runs in 2014-2016 has significantly enhanced the precision of open-heavy-flavor hadron measurements at STAR, while the Muon Telescope Detector has greatly improved muon identification and quarkonia measurements. Recent measurements from STAR on the dependence of jet modifications in heavy-ion collisions on the jet properties and medium geometry provide further insights into the parton energy loss in the QGP. The low p_T di-electron production is sensitive to the initial photon flux in heavy-ion collisions and can be a valuable tool to study the initial conditions in heavy-ion collisions. Some of the recent results from STAR on these and other related measurements, presented at the Hard Probes 2018 conference, are discussed in these proceedings.

International Conference on Hard and Electromagnetic Probes of High-Energy Nuclear Collisions
30 September - 5 October 2018
Aix-Les-Bains, Savoie, France

*Speaker.

1. Introduction

The STAR experiment [1] at RHIC is ideally suited to carry out measurements of the various hard and electromagnetic probes of the QGP (heavy flavor hadrons, jets, dileptons). Recently, for the RHIC runs in 2014-2016, STAR had installed a high-resolution silicon detector system, the Heavy Flavor Tracker (HFT) [2]. The HFT provides excellent vertex position resolution which significantly enhances the signal-to-background-ratio for the reconstruction of the open heavy flavor decays with very short life times. The other major detector upgrade at STAR was the Muon Telescope Detector (MTD) [3] which enhances muon identification and improves quarkonia measurements via decays to di-muons. STAR also has excellent charged particle tracking and particle identification capabilities with the Time Projection Chamber (TPC) and Time Of Flight (TOF) detector systems. The Barrel Electromagnetic Calorimeter (BEMC) enables to trigger on high p_T jets, photons, electrons and hadrons and aids in photon and electron identification.

In these proceedings, some of the recent results from STAR on the measurements of heavy flavor hadron production, flow, nuclear modification factor (R_{AA}), jet modification and energy loss, and low- p_T di-electron production in heavy-ion collisions, that were presented at the Hard Probes 2018 conference are discussed. Some of the results presented at the conference from STAR, but not discussed in these proceedings, include measurements of open bottom production in heavy-ion collisions, measurements of Υ suppression in heavy-ion collisions and cold nuclear matter effects in J/Ψ production, measurement of D^0 -hadron correlations, measurement of reaction-plane dependent away-side jet-like correlation shape, and use of machine learning methods in the measurement of the di-muon invariant mass spectrum in p+p collisions [4].

2. Heavy flavor production, flow and R_{AA}

2.1 Open heavy flavor production and R_{AA}

The charmed Lambda baryon, Λ_c^\pm , production can provide insights into the hadronization mechanism of charm quarks in the QGP. An enhancement of the $(\Lambda_c^+ + \Lambda_c^-)/(D^0 + \bar{D}^0)$ yield ratio (denoted by Λ_c/D^0 for the rest of the discussion) in heavy-ion collisions, compared to that in p+p collisions, is expected in the intermediate p_T region of $2 < p_T < 8$ GeV/c if the charm quarks hadronize via a coalescence mechanism [5]. Such an enhancement is observed for the baryon-to-meson ratio of light flavor hadrons and is attributed to the coalescence hadronization of the deconfined quarks in the QGP. Understanding the charm quark hadronization is also important for understanding the charm meson suppression and charm quark energy loss in the QGP.

The measurement of Λ_c^\pm production in Au+Au collisions at $\sqrt{s_{NN}} = 200$ GeV was carried out using the STAR data from 2014 and 2016, taken with the HFT. The Λ_c^\pm were reconstructed using the $\Lambda_c^\pm \rightarrow K^\mp \pi^\pm p^\pm$ channel. The supervised learning algorithm, Boosted Decision Trees (BDT), was used to improve the signal-to-background ratio. Figure 1 [6] shows the p_T and centrality dependence of the measured Λ_c/D^0 ratio in Au+Au collisions at mid-rapidity ($|\eta| < 1$). The Λ_c/D^0 ratio is found to be significantly enhanced in Au+Au collisions compared to the values from PYTHIA [7] calculations for p+p collisions. The model calculations with coalescence hadronization of charm quarks [5] show a similar enhancement as data and are able to qualitatively describe its p_T dependence, suggesting that coalescence plays a significant role in charm quark hadronization in the QGP. The measured Λ_c/D^0 ratio shows an increasing trend from peripheral to central

Au+Au collisions and the value measured in peripheral collisions is consistent with the value measured by ALICE in p+p collisions at $\sqrt{s} = 7$ TeV [9].

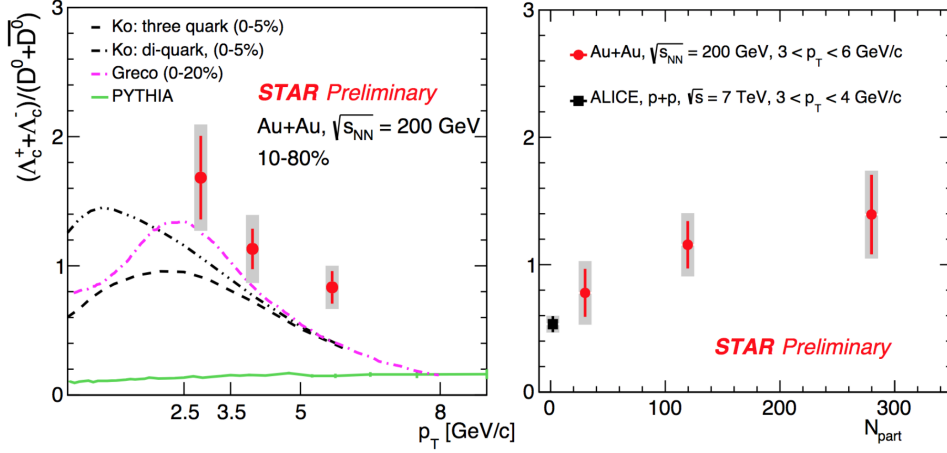


Figure 1: The Λ_c^\pm/D^0 ratio as a function of p_T for 10-80% centrality class (left) and as a function of N_{part} for $3 < p_T < 6$ GeV/c (right), in Au+Au collisions at $\sqrt{s_{\text{NN}}} = 200$ GeV. The error bars and gray bands represent statistical and systematic uncertainties, respectively.

The measurements of the R_{AA} and R_{CP} of D^0 mesons, using STAR data with the HFT from the Au+Au run at $\sqrt{s_{\text{NN}}} = 200$ GeV in 2014, are shown in figure 2 [6]. The data with HFT significantly improves the precision of the measurements compared to previously published results [10] and extends the measurements to zero p_T . The R_{AA} values are below unity at all p_T in central collisions. For $p_T > 5$ GeV/c, the D^0 R_{AA} shows significant suppression in central collisions, and the suppression decreases towards more peripheral collisions, as the system size decreases. The R_{CP} in the right panels of figure 2 is calculated relative to the 40-60% centrality class. The results for D^0 are also compared to the R_{CP} values for different light flavor hadrons in 200 GeV Au+Au collisions [9]. Similar levels of suppression are seen for D^0 and the light flavor hadrons for $p_T > 5$ GeV/c. Comparisons to two model calculations which incorporate both collisional and medium-induced radiative energy loss for charm quarks are also shown in the figure [11]. Both models can describe the data. The model parameters had been tuned to describe the previous STAR measurements [10]. The new high precision results reported here, along with the understanding of charm quark hadronization, can help better constrain the model parameters and the charm quark energy loss in the QGP.

In addition to the measurements of Λ_c^\pm and D^0 production, STAR has also measured the D_s^\pm and D^\pm yields [12] in 200 GeV Au+Au collisions. From these charm hadron yield measurements, we have extracted the $c\bar{c}$ production cross section per binary nucleon collision at midrapidity ($d\sigma^{c\bar{c}}/dy|_{y=0}$) in 200 GeV Au+Au collisions. While the D^0 yield is measured down to zero p_T , for the other charm hadron species, an extrapolation to zero p_T is used to calculate the total yield. The D^\pm and D_s^\pm spectra are extrapolated to zero p_T using Levy function fits. Fits using a power law function are used to estimate the systematic uncertainties from fitting. For Λ_c^\pm , the three model calculations shown in figure. 1 are used to extrapolate down to zero p_T . The mean value from the three fits is taken as the yield and the difference as systematics. The results are summarized in Table 1. The $c\bar{c}$ production cross section per binary nucleon collision at midrapidity measured

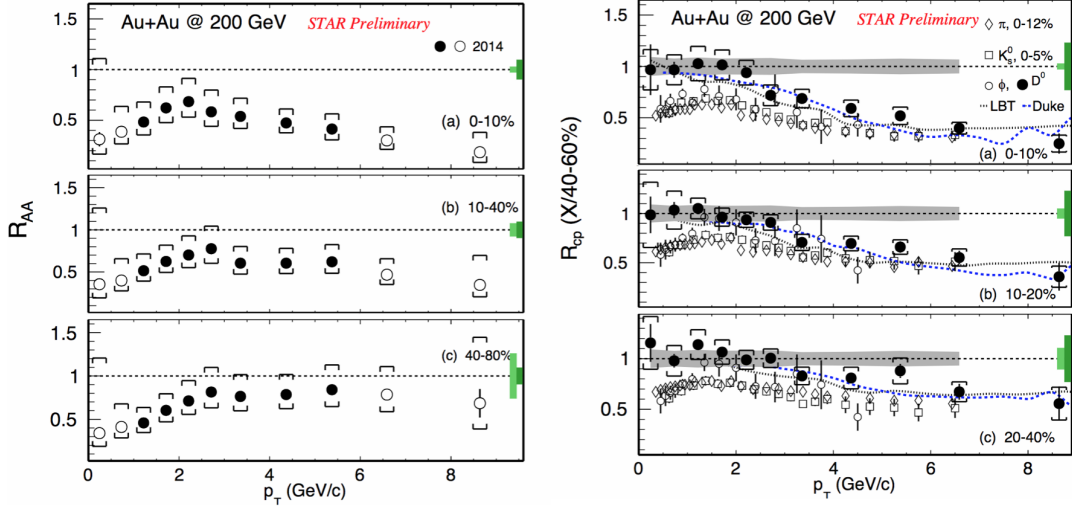


Figure 2: The D^0 R_{AA} (left) and R_{CP} values relative to 40-60% centrality class (right) as a function of p_T for different centrality intervals. The solid circles in the left panels indicate that measured p+p yields are used for calculating R_{AA} and the open circles indicate that the p+p yields from an extrapolation using a Levy fit to the measured yields are used. The error bars and brackets on the data points indicate statistical and systematic uncertainties respectively. The dark and light green boxes on the right of each panel show the global uncertainties. The shaded gray bands around unity on the R_{CP} plots indicate the uncertainty from vertex resolution correction for the 40-60% centrality class. [6]

in Au+Au collisions is consistent with that in p+p collisions [13] within uncertainties. However, the D^0 and D^\pm yields are suppressed, while those of Λ_c^\pm and D_s^\pm are enhanced, suggesting significant modifications to charm quark hadronization and hadrochemistry in the presence of the QGP medium.

	Charm hadron	Cross Section (μb)
Au+Au, 10-40%	D^0	41 ± 1 (stat) ± 5 (sys)
	D^\pm	18 ± 1 (stat) ± 3 (sys)
	D_s^\pm	15 ± 1 (stat) ± 5 (sys)
	Λ_c^\pm	78 ± 13 (stat) ± 28 (sys)
	$c\bar{c}$	152 ± 13 (stat) ± 29 (sys)
p+p	$c\bar{c}$	130 ± 30 (stat) ± 26 (sys)

Table 1: The charm hadron and $c\bar{c}$ production cross sections per binary nucleon collision at midrapidity in Au+Au and p+p collisions at $\sqrt{s_{NN}} = 200$ GeV.

2.2 Directed flow of D^0 mesons

The D^0 mesons exhibit large elliptic flow (v_2), comparable in magnitude to those of light flavor hadrons in Au+Au collisions, suggesting strong interactions of the charm quarks with the QGP [14]. Recent theoretical calculations also predict a significant directed flow (v_1) for D^0 mesons [15]. The D^0 v_1 is predicted to be an order of magnitude larger than that for light flavor hadrons, arising from the interactions of the charm quarks with the tilted medium [16] of soft particles. The left panel of figure 3 [17] shows the measurement of the combined D^0 and \bar{D}^0 v_1 in Au+Au collisions at $\sqrt{s_{NN}} = 200$ GeV. The measurements were carried out using the data recorded by STAR (with the HFT) experiment during RHIC runs in 2014 and 2016. The first order event plane is determined

using the spectator neutrons detected by the Zero Degree Calorimeters [1] which are situated at far forward rapidities ($|\eta| > 6.3$). The v_1 signal is calculated using the event plane method [14] correlating D^0 and \bar{D}^0 yields at mid-rapidity with the first order event plane, and corrected for the event plane resolution. The measured slope of D^0 v_1 at mid-rapidity ($dv_1/dy|_{y=0}$) is found to be significantly larger compared to that for the light flavor hadrons. Model calculations [15] based on charm quark transport in a hydrodynamic medium, with tilted initial conditions for the medium, predict the correct sign and a similar order of magnitude for the D^0 v_1 . The measurements can help further constrain the charm quark transport in the QGP. The right panel of figure 3 shows the v_1 for D^0 and \bar{D}^0 separately. It is also predicted that the difference between D^0 and \bar{D}^0 is sensitive to the initial strong electro-magnetic fields in heavy-ion collisions [18]. The measured $dv_1/dy|_{y=0}$ for D^0 and \bar{D}^0 are consistent with each other, within the sizeable uncertainties of the current measurement.

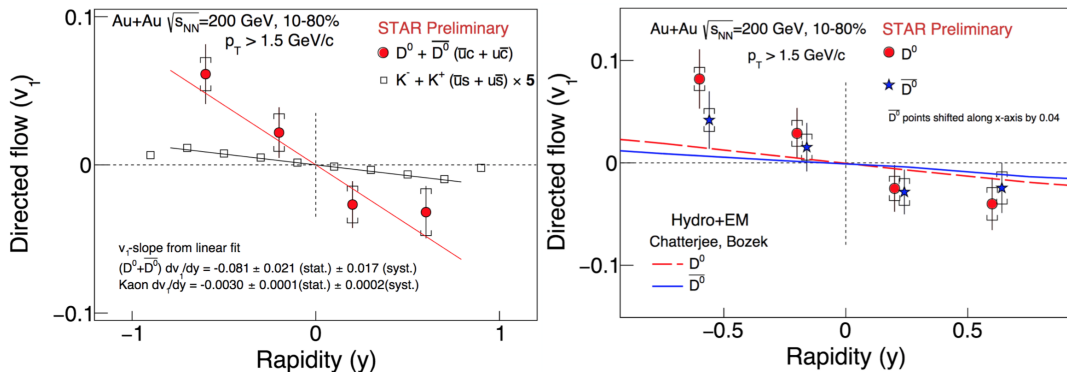


Figure 3: (Left) The directed flow v_1 for the combined D^0 and \bar{D}^0 hadrons (solid circles) for $p_T > 1.5$ GeV/c in 10-80% central Au+Au collisions compared to that of kaons (open squares). The solid lines are linear fits to data. (Right) The v_1 for D^0 and \bar{D}^0 shown separately and compared to model calculations (solid and dashed lines). The error bars in both panels indicate statistical uncertainties and the brackets indicate systematic uncertainties.

3. Jet modification and energy loss

3.1 Dependence of di-jet asymmetry on jet properties and jet angular resolution

STAR previously published [19] measurements of the di-jet asymmetry in Au+Au and p+p collisions, defined as $A_J = (p_T^{\text{lead}} - p_T^{\text{sublead}})/(p_T^{\text{lead}} + p_T^{\text{sublead}})$, p_T^{lead} and p_T^{sublead} being the p_T of the leading and subleading jets, respectively. It was seen that for the “hard-core” jets reconstructed by clustering only the hard constituents (by applying a hard constituent p_T cut, $p_T^{\text{hard-const}} > 2$ GeV/c) of the event, the A_J distributions were significantly modified in Au+Au collisions compared to those in p+p collisions for (anti- k_T) jets of radius $R = 0.4$. The A_J distributions were also studied for the “matched jets” formed by reclustering the constituents in the event with a much lower constituent p_T cut ($p_T^{\text{matched-const}} > 0.2$ GeV/c), and required to be geometrically matched to a hard-core jet ($\Delta R < 0.4$). The A_J distributions were found to be consistent between p+p and Au+Au for the matched jets with $R = 0.4$, i.e when including the soft contribution within the jet radius of 0.4.

The analysis is extended to study the dependence of A_J distributions on the jet radius and the hard-core constituent p_T cut. The analysis is carried out using Au+Au and p+p data collected by STAR at $\sqrt{s_{NN}} = 200$ GeV. The p+p data is embedded into Au+Au events of same centrality to account for background fluctuations and reconstruction inefficiencies [20]. The leading and

subleading jets are required to have $p_T^{\text{lead}} > 16 \text{ GeV}/c$ and $p_T^{\text{sublead}} > 8 \text{ GeV}/c$ respectively, and required to be back-to-back in ϕ with $|\phi^{\text{lead}} - \phi^{\text{sublead}} - \pi| < 0.4$. The jet radius R is varied between 0.2 to 0.4 and the $p_T^{\text{hard-const}}$ cut between 1 GeV/c and 3 GeV/c . It is found that at R of 0.2 the A_J distributions for matched jets in Au+Au are more imbalanced than those in p+p, for all choices of $p_T^{\text{hard-const}}$ cuts. As R is increased, the A_J distributions for matched jets became more consistent between Au+Au and p+p. It is also found that for higher $p_T^{\text{hard-const}}$ cuts ($> 2 \text{ GeV}/c$), the A_J distributions at larger jet-radius became consistent between Au+Au and p+p, while for lower $p_T^{\text{hard-const}}$ values ($\sim 1 \text{ GeV}/c$), they remained less consistent even for jets with $R = 0.4$. Thus by modifying the di-jet definition used during jet-finding, we can select jets that are relatively more or less modified compared to a p+p reference. This opens up the possibility of jet geometry engineering, and may help constrain the path length dependence of partonic energy loss in the QGP at RHIC.

Jet-medium interaction can be dependent on the resolution scale or the coherence length of the medium, that determines if the jet is seen by the medium as a single radiating object or a multi-pronged one [21]. The dependence of the jet modification in Au+Au collisions on the jet angular scale is studied [22]. The constituents of an anti- k_T jet of $R = 0.4$ are reclustered into an inclusive set of anti- k_T sub-jets (SJ) of $R = 0.1$. A minimum sub-jet p_T requirement of 2.97 GeV/c is enforced in central Au+Au collisions to reduce sensitivity to the background fluctuations. The angular distance between the leading (SJ1) and subleading (SJ2) sub-jet axes, $\theta_{SJ} = \Delta R(SJ1, SJ2)$, is used to characterize the jet angular scale. The di-jet asymmetry (A_J) distributions are then studied for jets with different θ_{SJ} values. The trigger and recoil jets were required to have $p_T > 16 \text{ GeV}/c$ and $p_T > 8 \text{ GeV}/c$, respectively, as in the previous study. Figure 4 shows the A_J distributions for two different choices of θ_{SJ} values, for hard-core jets and matched jets. The hard-core jets show significant modification of the A_J distributions in Au+Au compared to that from p+p data embedded into Au+Au, for both small and large θ_{SJ} selections. The A_J distributions for matched jets recover the balance to level seen in p+p collisions for both θ_{SJ} selections. This is similar to the observations from θ_{SJ} independent studies [19], indicating no apparent distinction between large θ_{SJ} and small θ_{SJ} jets by the medium at RHIC energies.

3.2 Direct-photon triggered jets

Measurements of recoil jets to a direct-photon (γ_{dir}) trigger (γ_{dir} +jet) are valuable probes of the parton energy loss in the QGP [23]. The γ_{dir} , being colorless, does not lose energy in the QGP and thus narrowly constrains the initial energy of the recoil parton (predominantly a quark from QCD Compton scattering) energy. The recoil jets to a π^0 hadron trigger (π^0 +jet) can be from a quark or gluon and thus complement the measurements of γ_{dir} +jet. The measurements were carried out using Au+Au and p+p collisions at $\sqrt{s_{NN}} = 200 \text{ GeV}$, for the 0-15% most central Au+Au collisions [26]. A Transverse Shower Profile method [24] was used to discriminate between π^0 and γ_{rich} -triggers. Here γ_{rich} represents an enriched sample of γ_{dir} with an admixture of photons from π^0 decays. The purity of γ_{dir} in the γ_{rich} triggered sample varies between 65%-85% for the trigger range of $9 < E_T^{\text{trig}} < 20 \text{ GeV}$. Charged jets were reconstructed using anti- k_T algorithm with constituents required to have $0.2 < p_T < 15 \text{ GeV}/c$. The recoil-jet region is defined as $\Delta\phi \in [\pi - \pi/4, \pi + \pi/4]$. Semi-inclusive charged recoil-jet p_T distributions are constructed for a given E_T^{trig} range for γ_{dir} and π^0 triggers. The uncorrelated background yield to the recoil jet distributions

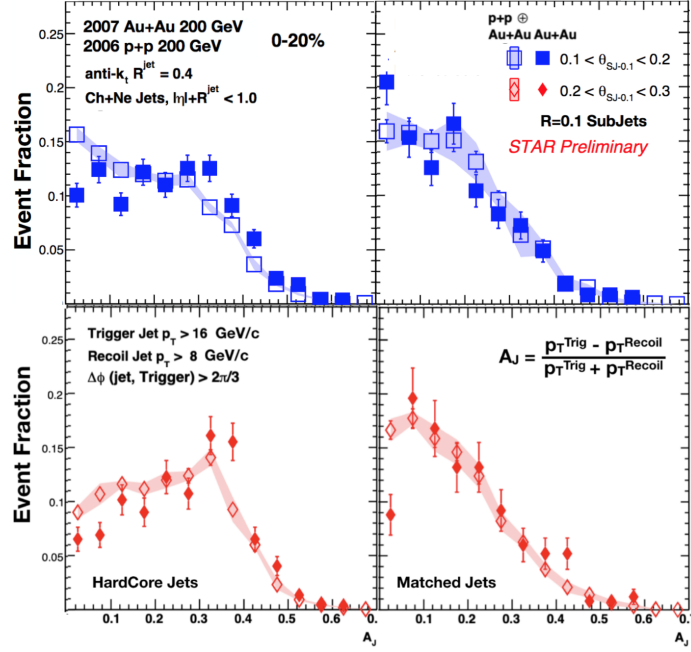


Figure 4: The A_J distributions for hard-core jets (left) and matched jets (right) for jets with small θ_{Sj} values (top panels) and with large θ_{Sj} values (lower panels). The solid symbols are for distributions for Au+Au data and open symbols for p+p data embedded into Au+Au. Error bars and shaded band represent statistical and systematic uncertainties, respectively.

is determined using an event-mixing technique [25]. After subtraction of the background yield, recoil-jet p_T distributions are then corrected for detector effects and are also corrected for the γ_{dir} purity for the γ_{dir} +jet measurements.

The suppression of the recoil jet yield in Au+Au collisions is quantified relative to that in p+p collisions calculated from PYTHIA using the ratio $I_{AA}^{\text{PYTHIA}}(p_T^{\text{ch}}) = Y^{\text{Au+Au}}(p_T^{\text{ch}})/Y^{\text{PYTHIA}}(p_T^{\text{ch}})$, where $Y^{\text{Au+Au}}$ and Y^{PYTHIA} denote the per-trigger yield of the recoil jets in Au+Au and PYTHIA, respectively. Figure 5 shows the $I_{AA}^{\text{PYTHIA}}(p_T^{\text{ch}})$ for γ_{dir} +jet and π^0 +jet, for a trigger bin of $11 < E_T^{\text{trig}} < 15$ GeV. Strong suppression is observed for both γ_{dir} +jet and π^0 +jet yields. The extents of the observed suppression are similar between the γ_{dir} +jet and π^0 +jet yields, consistent within the systematic uncertainties of the measurements.

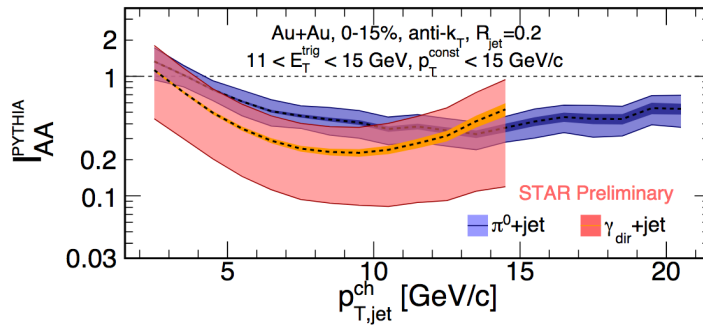


Figure 5: The $I_{AA}^{\text{PYTHIA}}(p_T^{\text{ch}})$ values for γ_{dir} +jet and π^0 +jet yields for a trigger bin of $11 < E_T^{\text{trig}} < 15$ GeV. Lighter and darker bands represent systematic and statistical uncertainties, respectively.

4. Low p_T di-electron production in Au+Au collision

In heavy-ion collisions, dileptons can be produced from photon-photon interactions from the large flux of quasi-real photons generated by the strong electro-magnetic fields in these collisions [27]. The dileptons produced from these photon-photon interactions are known to distinctively peak at low p_T . Measurements of the low p_T e^+e^- production in different collision systems with nuclear overlap are essential to constrain the photon-photon interactions in heavy-ion collisions. The measurements [28] are carried out using data from Au+Au collisions at $\sqrt{s_{NN}} = 200$ GeV and U+U collisions at $\sqrt{s_{NN}} = 193$ GeV. The distributions of the like sign pairs, corrected for acceptance differences between like and unlike sign pairs, are used to subtract combinatorial and correlated background. The raw signal distributions of e^+e^- pairs, after the background subtraction, are corrected for the detector efficiency.

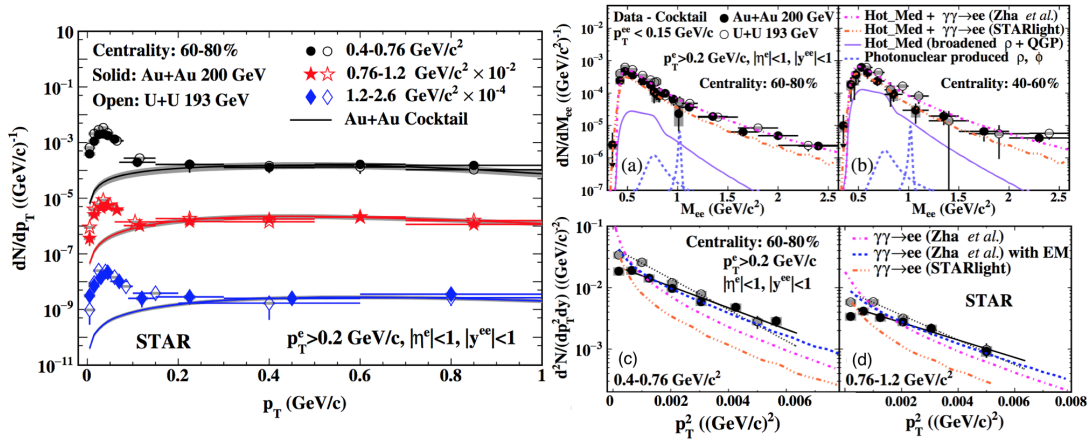


Figure 6: (Left) The e^+e^- pair p_T distributions within the STAR acceptance for 60-80% Au+Au and U+U collisions compared to hadronic cocktail for three invariant mass regions. (Right panels (a) and (b)) The low p_T mass spectra for the e^+e^- excess above the hadronic cocktail for 60-80% and 40-60% Au+Au and U+U events. (Right panels (c) and (d)) The p_T^2 distributions for the excess yields for 60-80% Au+Au and U+U collisions for the invariant mass regions 0.4-0.76 GeV/c² and 0.76-1.2 GeV/c². The gray boxes on the data points and the shaded band on the cocktail curves indicate systematic uncertainties.

The left panels of figure 6 show the p_T distributions of efficiency corrected e^+e^- pair yields in three invariant mass regions for Au+Au and U+U collisions in the 60-80% centrality bin. The hadronic cocktail that takes into account the contributions from known hadronic sources describes the data well for $p_T > 0.15$ GeV/c in all three mass regions. The right panels (a) and (b) of figure 6 show the integrated yield in $p_T < 0.15$ GeV/c above the hadronic cocktail, as a function of the di-electron invariant mass. The models for photon-photon interactions from the initial photon flux, STARlight [29] and the model by Zha *et al.* [30] can describe the measured excess yields. The right panels (c) and (d) show the p_T^2 ($\approx -t$, the squared momentum transfer) distributions of the e^+e^- excess yields in $p_T < 0.15$ GeV/c for two invariant mass regions in 60-80% central collisions. The STARlight and model from Zha *et al.*, that can describe the measured excess yields in $p_T < 0.15$ GeV/c, fail to describe its p_T^2 distribution. Calculations that further include the p_T broadening to di-electron pairs passing 1 fm through a strong magnetic field (10^{14} T) trapped in the QGP [31], can describe the p_T^2 distributions better. This may indicate the possible existence of a strong magnetic field trapped in the conducting QGP, however systematics of the model calculations for photon-

photon interactions, including their impact parameter dependence, need to be understood better to draw strong conclusions.

5. Summary

A subset of the recent results from STAR shown at the Hard Probes 2018 conference is presented. The open charm hadron measurements indicate strong interactions of the charm quarks with the QGP medium and suggest that charm quarks hadronize via a coalescence mechanism in heavy-ion collisions at RHIC. These measurements will help better constrain the charm quark energy loss in the QGP. We also find that while the extracted per-nucleon charm cross-section at mid-rapidity in Au+Au collisions is consistent with that in p+p collisions, the charm hadrochemistry is significantly modified compared to that in p+p collisions. The dependence of the modifications of the di-jet asymmetry distributions in Au+Au collisions on the jet radius, hard constituent p_T cut and the jet angular resolution is studied. The first fully corrected γ_{dir} +jet measurements at RHIC is also presented. Model calculations with photon-photon interactions from the initial photon flux describe the yields of the low p_T (< 0.15 GeV/c) di-electron excess above the hadronic cocktail in peripheral Au+Au and U+U collisions, but fail to describe the p_T^2 distributions. This additional p_T broadening could be from the strong magnetic fields present in heavy-ion collisions, making low p_T dileptons a valuable tool to study the initial conditions in heavy-ion collisions.

References

- [1] K. H. Ackermann *et al.* Nucl. Instrum. Meth. A **499** 624-632 (2003).
- [2] G. Contin *et al.*, Nucl. Inst. Meth. A **907** 60-80 (2018).
- [3] L. Ruan *et al.* J. Phys. G **36** 095001 (2009).
- [4] X. Chen (STAR Collaboration), these proceedings; Z. Liu (STAR Collaboration), these proceedings; A. Jentsch (STAR Collaboration), these proceedings; L. Zhang (STAR Collaboration), these proceedings; D. Brandenburg (STAR Collaboration), these proceedings
- [5] Y. Oh *et al.*, Phys. Rev. **C79**, 044905 (2009); S. H. Lee *et al.*, Phys. Rev. Lett. **100**, 222301 (2008); S. Ghosh *et al.*, Phys. Rev. **D90(5)**, 2-7 (2014).
- [6] G. Xie (STAR Collaboration), these proceedings
- [7] T. Sjostrand, S. Mrenna and P. Skands, Journal of High Energy Physics **2006**, 026 (2006).
- [8] ALICE Collaboration, Journal of High Energy Physics **04** 108 (2018).
- [9] STAR Collaboration, Phys. Rev. Lett. **97**, 152301 (2006); Phys. Rev. C **79**, 064903 (2009); Phys. Rev. Lett. **108**, 072301
- [10] STAR Collaboraion, Phys. Rev. Lett. **113**, 142301, (2014).
- [11] Y. Xu *et al.* Phys. Rev. C. **97**, 014907 (2018); S. Cao *et al.*, Phys. Rev. C **94**, 014909 (2016).
- [12] L. Zhou (STAR Collaboration) Nucl. Phys. A. **967**, 620-623 (2017); J. Vanek (STAR Collaboration) Quark Matter 2018 Poster <https://indico.cern.ch/event/656452/contributions/2859701/>
- [13] STAR Collaboration, erratum for Phys. Rev. Lett. **113**,142301 (2014).
- [14] L. Adamczyk *et al.* (STAR Collaboration), Phys. Rev. Lett. **118**, 212301 (2017).
- [15] S. Chatterjee and P. Bozek, Phys. Rev. Lett. **120**, 192301 (2018).
- [16] P. Bozek and I. Wyskiel, Phys. Rev. C **81**, 054902 (2010).
- [17] L. He (STAR Collaboration), these proceedings
- [18] S. Das *et al.*, Phys. Lett.B **768**, 260 (2017).
- [19] L. Adamczyk, *et al.*, Phys. Rev. Lett. **119(6)** 062301 (2017)
- [20] N. Elsey (STAR Collaboration), these proceedings
- [21] Y. Mehtar Tani and K. Tywoniuk, Phys. Rev. D **98**, 051501 (2018) (R)
- [22] R. Elayavalli (STAR Collaboration), these proceedings
- [23] X.-N. Wang *et al.*, Phys. Rev. Lett. **111**, 062301 (2013); H. Zhang *et al.*, Phys. Rev. Lett. **103**, 032302 (2009).
- [24] L. Adamczyk *et al.* (STAR Collaboration), Phys. Lett. B, **760** 689-696 (2016).
- [25] L. Adamczyk *et al.* (STAR Collaboration), Phys. Rev. C **96** no.2, 024905 (2017).
- [26] N. Sahoo (STAR Collaboration), these proceedings
- [27] G. Baur *et al.*, Phys. Rep. **364**, 359 (2002); C. A. Bertulani *et al.*, Annu. Rev. Nucl. Part. Sci., **271** (2005).
- [28] J. Adam *et al.* (STAR Collaboration), Phys. Rev. Lett. **121**, 132301 (2018).
- [29] S. R. Klein *et al.*, Comput. Phys. Commun. **212**, 258 (2017).
- [30] W. M. Zha *et al.*, Phys. Lett. B **781**, 182 (2018).
- [31] D. E. Kharzeev and H. J. Warringa, Phys. Rev. D **80**, 034028 (2009).